Rapid Communications

Corbino magnetoresistance in ferromagnetic layers: Two representative examples $Ni_{81}Fe_{19}$ and $Co_{83}Gd_{17}$

B. Madon and J.-E. Wegrowe*
Laboratoire des Solides Irradiés, Ecole Polytechnique, CNRS, CEA, Université Paris-Saclay, F-91128 Palaiseau, France

M. Hehn, F. Montaigne, and D. Lacour
Institut Jean Lamour, UMR 7198, CNRS, Université de Lorraine, Vandoeuvre les Nancy, France

(Received 21 July 2018; revised manuscript received 26 November 2018; published 12 December 2018)

The magnetoresistance of $Ni_{81}Fe_{19}$ and $Co_{83}Gd_{17}$ ferromagnetic thin films is measured in Corbino disk geometry, and compared to the magnetoresistance of the same films measured in the Hall-bar geometry. The symmetry of the magnetoresistance profiles is drastically modified by changing the geometry of the sample, i.e., by changing the boundary conditions. These properties are explained in a simple model, showing that the Corbino magnetoresistance is defined by the potentiostatic boundary conditions while the Hall-bar magnetoresistance is defined by galvanostatic boundary conditions.

DOI: 10.1103/PhysRevB.98.220405

The Hall effect was first measured in 1879 by Hall [1] by applying a magnetic field to a conducting slab contacted to an electric generator at the extremities. Later on, Corbino [2] found a similar effect by applying a magnetic field on a disk geometry with two concentric electrodes. Quickly the question arose on whether the effect measured by Corbino (the so-called Corbino effect) in a disk and by Hall in a bar have the same origin. In 1914, Adams and Chapman measured the Corbino effect in many different metals [3] by using an oscillating current flowing from the center of the disk to its outer. Adams concluded in 1915 that "the Corbino effect is, essentially, the same as the Hall effect" [4]. However, the question remains about the exact meaning of the adverb "essentially."

In the 1950's, the Hall effect in the Corbino geometry was studied for its practical applications. The magnetoresistance of InSb slabs was shown to depend strongly on the shape of the samples [5]. The reason is that near the current injection edge, the Hall electric field is shorted and a transverse electric current appears which causes an increase of the resistance as in the Corbino geometry [6–9]. Accordingly, one can see the Corbino geometry as the extreme scenario where the Hall electric field is zero everywhere and a Hall current is flowing, or, in other terms, one can view the Corbino disk as a Hall bar in which the electrostatic charge accumulation is reduced to zero everywhere. The system cannot generate a voltage between the edges so that a Hall current is flowing and the Joule heating is higher than in the Hall bar for an equivalent volume [10–12]. The mechanism responsible for both the Hall effect and the Corbino effect is indeed the same, but the Corbino disk is a device that is more constrained than the Hall bar, due to the change of the boundary conditions.

At the turn of the last century, the emergence of spintronics has shown the possibility of exploiting spin-polarized currents and spin-dependent potentials, and has paved the way to the realization of new electronic devices. Recently, various developments about the spin-Hall effects (anomalous Hall effect, spin-Hall effect, spin-pumping effect, spin-Seebeck effects, etc. [13,14]) tend to show that the usual Hall-bar conditions with spin relaxation could be turned into "Corbino-like boundary conditions," in the sense that the electric charge accumulation drops to zero at the edges and a pure spin current can be generated instead of a Hall voltage [11].

In this context, the goal of this Rapid Communication is to study NiFe and GdCo ferromagnetic Corbino disks and Hall bars, in order to understand the behavior of the magnetoresistance [13,15–17] when the boundary conditions are switched (by changing the geometry) from spin current to spin-dependent voltage. The alloys $Ni_{81}Fe_{19}$ and $Co_{83}Gd_{17}$ are chosen for their maximum contribution to the anisotropic magnetoresistance and the anomalous Hall magnetoresistance (that defines the anomalous Hall angle), respectively.

First, we will present our measures of Corbino magnetoresistance performed on NiFe and CoGd rings. The results are then analyzed in the framework of the generalized Ohm's law by defining the *Corbino magnetotransport coefficients* $\mathcal{C}$ as a function of the usual Hall-bar coefficients [see Eq. (12) below]. The consistency of the proposed explanation is checked independently, by measuring the magnetotransport coefficients of the Hall bar.

The samples studied are 20-nm-thick layers of $Ni_{81}Fe_{19}$ and $Co_{83}Gd_{17}$ sputtered on glass substrates. The magnetic layers are sandwiched between 5-nm-thick Ta buffers and 3-nm-thick Pt caps. The magnetic properties of the thin layers have been previously studied [18] (see Supplemental Material [19]). The sample magnetization is uniform for quasistatic states, although nonuniform states could take place at low magnetic fields (this regime is, however, not considered in the present study). The NiFe is textured with small uniaxial anisotropy lying in the sample plane. The coercivity field in the in-plane geometry is of the order of 1 mT. The out-

*jean-eric.wegrowe@polytechnique.edu

 ©2018 American Physical Society

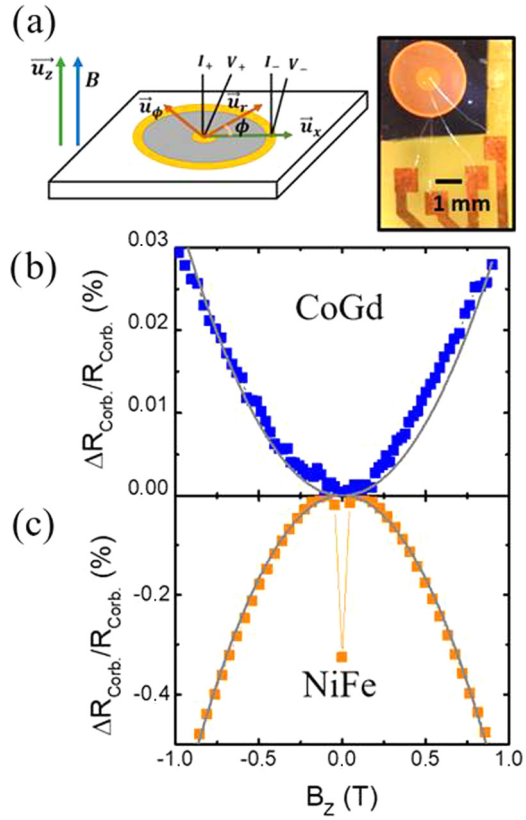

FIG. 1. (a) Schematic view of the Corbino geometry, with the three unit vectors $\vec{u}_r, \vec{u}_\phi, \vec{u}_x$ confined in the plane. (b) and (c) Corbino magnetoresistances for the CoGd and NiFe samples measured as a function of the out-of-plane magnetic field. The gray lines are a quadratic fitting of the data.

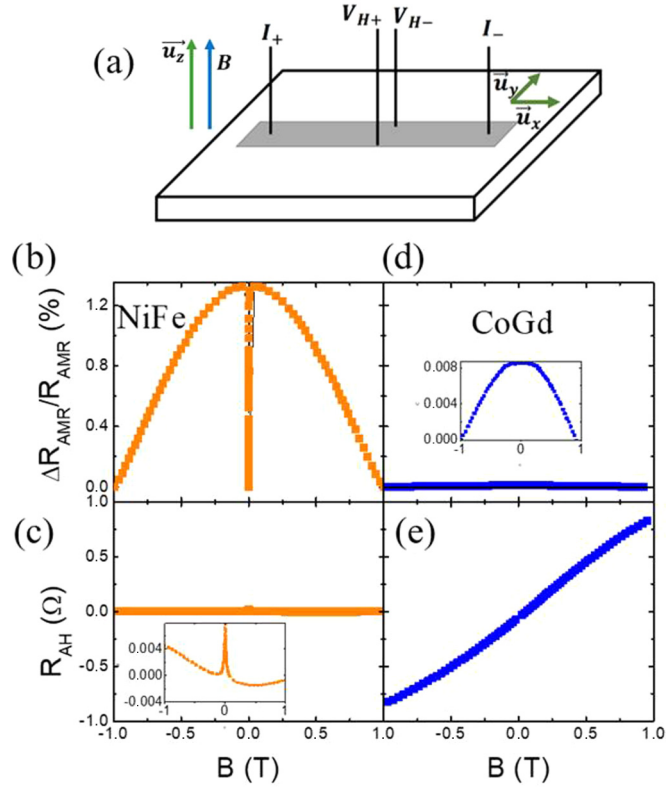

FIG. 2. (a) Schematic view of the Hall-bar devices. Resistance measurements vs applied field for the NiFe device in the (b) longitudinal and (c) transverse geometries. Resistance measurements vs applied field for the CoGd device in the (d) longitudinal and (d) transverse geometries. The two insets are zooms (magnification 100×).

of-plane shape anisotropy corresponds to a field of about 1 T, defined by the magnetization at saturation $M_s(\text{NiFe}) \approx 800$ emu cm^{-3}. The CoGd has a comparable magnetization, with a similar shape anisotropy. The structure of CoGd is amorphous and it is not textured. Owing to a standard two-step UV lithographic process, they have been patterned in Corbino rings with an inner and outer radius respectively equal to 7 and 2 mm. Gold contact pads are formed in the second step. Figure 1(a) presents a sketch of the obtained devices.

The measured magnetoresistance of NiFe and CoGd Corbino rings is presented respectively in Figs. 1(b) and 1(c). The voltage is measured as a function of the current with a current swept from -1 to $+1$ mA. The resistance is deduced by fitting the $I(V)$ curve in order to eliminate thermoelectric contributions. In both materials, an increasing magnetic field leads to *parabolic magnetoresistance*. The nonparabolic point at zero magnetic field in Fig. 1(c) corresponds to the variation observed in Fig. 2(b) and is due to the small in-plane anisotropy for the NiFe sample [19]. Note that while a negative Corbino magnetoresistance is measured for NiFe devices, it is positive in the CoGd case. It is also remarkable that the amplitude of the NiFe Corbino signal is one order of magnitude higher than the one measured in the CoGd case.

To shed light on these Corbino magnetoresistance profiles and the drastic differences between NiFe and CoGd, it is necessary to have a look at the Ohm's law $\vec{E} = \bar{\bar{\rho}}\vec{J}$ generalized to ferromagnetic conductors. The resistivity tensor $\bar{\bar{\rho}}$ contains both anisotropic terms and anomalous Hall terms [15,17] (see Supplemental Material [19]). In the Hall-bar geometry, a current is imposed along the x axis and the device is in a *galvanostatic mode*: We then use the resistivity representation of the Ohm's law,

$$\vec{E} = \rho\vec{J} + \Delta\rho(\vec{m}\cdot\vec{J})\vec{m} + \rho_{\text{AH}}\vec{m}\times\vec{J}, \qquad (1)$$

where $\vec{m}$ is the magnetization normalized to unity and $\vec{E}$ is the electric field. The first coefficient ρ on the right-hand side is the isotropic resistivity and it accounts for isotropic transport. The second term is the anisotropic magnetoresistance described by the the coefficient $\Delta\rho/\rho$, where $\Delta\rho = \rho_\parallel - \rho_\perp$ is the difference between the resistivity measured with a current parallel to the magnetization $\rho_\parallel$ and the resistivity measured with a current perpendicular to the magnetization $\rho_\perp$ ($\Delta\rho/\rho$ is positive). The last term is the anomalous Hall magnetoresistance described by the anomalous Hall resistivity ρ_{AH} (as discussed in the Supplemental Material [19], the coefficient ρ_{AH} plays the same role as the Hall resistivity [13,20,21]).

In the following, we describe the magnetization $\vec{m}$ in Cartesian coordinates $\vec{m} = m_x\vec{u}_x + m_y\vec{u}_y + m_z\vec{u}_z$ with the set of unit vectors $\{\vec{u}_x, \vec{u}_y, \vec{u}_z\}$ in the case of Hall bars, while it is described in cylindrical coordinates $\vec{m} = m_r\vec{u}_r + m_\phi\vec{u}_\phi + m_z\vec{u}_z$ with the set of unit vectors $\{\vec{u}_r, \vec{u}_\phi, \vec{u}_z\}$ in the case of

Corbino disks [see Fig. 1(a)]. In this last case, the boundary conditions are such that the potential V_0 is imposed in the inner disk while the outer disk is set at the ground. The device is then in a *potentiostatic mode*. The resistance is given by the ratio V_0/I, where the current is the integral of the radial current densities over the angle ϕ and the thickness t of the disk,

$$I(r) = \int_{z=0}^{t} \int_{\phi=0}^{2\pi} J_r(r,\phi) r \, d\phi \, dz. \tag{2}$$

In this potentiostatic mode, it is convenient to inverse Eq. (1) in order to use the conductivity representation [8]. The Ohm's law now reads $\vec{J} = \overline{\overline{\sigma}}\vec{E}$, where the conductivity tensor $\overline{\overline{\sigma}} = (\overline{\overline{\rho}})^{-1}$ is the inverse of the resistivity tensor $\overline{\overline{\rho}}$ used in Eq. (1). We then have the current as a function of the electric field,

$$\vec{J} = \sigma\vec{E} + \Delta\sigma(\vec{m}\cdot\vec{E})\vec{m} - \sigma_{\mathrm{AH}}\vec{m}\times\vec{E}, \tag{3}$$

where the three conductivity coefficients are related to the three resistivity coefficients by the relations

$$\sigma = \frac{\rho}{\rho^2+\rho_{\mathrm{AH}}^2}, \quad \Delta\sigma = \frac{1}{\rho+\Delta\rho} - \frac{\rho}{\rho^2+\rho_{\mathrm{AH}}^2}, \quad \sigma_{\mathrm{AH}} = \frac{\rho_{\mathrm{AH}}}{\rho^2+\rho_{\mathrm{AH}}^2}. \tag{4}$$

As shown in the following, this simple inversion between Eqs. (1) and (3) is responsible for the considerable change observed in the magnetoresistance profiles between the Corbino disk (Fig. 1) and the Hall bar (Fig. 2).

The striking specificity of the Corbino geometry is the absence of charge accumulation (since the two opposite edges of the Hall bar are contacted together in the Corbino disk). As a consequence, the Poisson equation reduces to the Laplace equation $\nabla^2 V = 0$, which leads to the following form of the electric potential,

$$V(r) = V_0\left(1 - \frac{\ln(r/r_{\mathrm{in}})}{\ln(r_{\mathrm{out}}/r_{\mathrm{in}})}\right), \tag{5}$$

where r_{in} is the inner disk radius, and r_{out} is the outer disk radius. This leads to the planar component of the electric field,

$$\vec{E} = -\vec{\nabla}V = \frac{V_0}{\ln(r_{\mathrm{out}}/r_{\mathrm{in}})}\frac{1}{r}\vec{u}_r. \tag{6}$$

Furthermore, an out-of plane electric field E_z is introduced in order to take into account the thickness of the sample. Since the difference $r_{\mathrm{out}} - r_{\mathrm{in}}$ between the radius of the inner disk and the outer disk is much larger than the thickness t of the layer, we assume that E_z is uniform and the out-of-plane component of the current is zero. Consequently, the electric field and electric current read

$$\vec{E} = \begin{pmatrix} \frac{V_0}{\ln(r_{\mathrm{out}}/r_{\mathrm{in}})}\frac{1}{r} \\ 0 \\ E_z \end{pmatrix}_{r,\phi,z} \quad \text{and} \quad \vec{J} = \begin{pmatrix} J_r \\ J_\phi \\ 0 \end{pmatrix}_{r,\phi,z}. \tag{7}$$

Introducing relations (7) in Eq. (3), we obtain a system of three equations with the three unknowns $\{J_r, J_\phi, E_z\}$. We set the x axis as the direction of the in-plane component of the magnetization. Using $m_r^2 + m_\phi^2 + m_z^2 = 1$, and the relation $m_\phi^2 = (1-m_z^2)\sin^2\phi$, we obtain

$$J_r(r,\phi) = \frac{\sigma^2 + \Delta\sigma\sigma + \sin^2\phi\left(\sigma_{\mathrm{AH}}^2 - \sigma\Delta\sigma\right)\left(1-m_z^2\right)}{\sigma + \Delta\sigma m_z^2}\frac{V_0}{\ln(r_{\mathrm{out}}/r_{\mathrm{in}})}\frac{1}{r}. \tag{8}$$

Integrating according to Eq. (2) and dividing by the current gives the Corbino resistance,

$$R_{\mathrm{Cor}} = \frac{V_0}{I} = \frac{\ln(r_{\mathrm{out}}/r_{\mathrm{in}})}{\pi t}\frac{\sigma + \Delta\sigma\left(1-m_z^2\right)}{2\sigma^2 + 2\Delta\sigma\sigma + m_z^2\left(\sigma_{\mathrm{AH}}^2 - \sigma\Delta\sigma\right)}. \tag{9}$$

To obtain R_{Cor} as a function of the resistivity coefficients ρ, $\Delta\rho$, and ρ_{AH} that are usually measured, we insert Eqs. (4) into Eq. (9) and we obtain

$$R_{\mathrm{Cor}}(m_z) = \frac{\ln(r_{\mathrm{out}}/r_{\mathrm{in}})}{2\pi t}\rho\frac{1 + \Delta\rho/\rho\left(1-m_z^2\right) + \rho_{\mathrm{AH}}^2 m_z^2/\rho^2}{1 + \Delta\rho/(2\rho)\left(1-m_z^2\right)}. \tag{10}$$

Considering that $\Delta\rho/\rho \ll 1$ (this is the case for the materials used in this study) the magnetoresistance defined as $\Delta R_{\mathrm{Cor}}(m_z)/R_{\mathrm{Cor}} \equiv [R_{\mathrm{Cor}}(m_z) - R_{\mathrm{Cor}}(0)]/R_{\mathrm{Cor}}(0)$ can finally be expressed as

$$\frac{\Delta R_{\mathrm{Cor}}(m_z)}{R_{\mathrm{Cor}}} = \left[\left(\frac{\rho_{\mathrm{AH}}}{\rho}\right)^2 - \frac{\Delta\rho}{2\rho}\right]m_z^2. \tag{11}$$

Accordingly, for ferromagnetic devices patterned in the Corbino geometry we expect a Corbino magnetoresistance proportional to m_z^2. This is qualitatively in agreement with the trend measured in Figs. 1(b) and 1(c). Quantitatively, the prefactor on the right-hand side of Eq. (11)—the *Corbino coefficient*—which is defined by

$$\mathcal{C} = \left(\frac{\rho_{\mathrm{AH}}}{\rho}\right)^2 - \frac{\Delta\rho}{2\rho}, \tag{12}$$

is the difference between the square of the anomalous Hall magnetoresistance and half the anisotropic magnetoresistance. The positive parabolic profile then corresponds to a dominance of the anomalous Hall magnetoresistance, while the negative parabolic profile corresponds to a dominance of the anisotropic magnetoresistance.

In order to verify the validity of Eq. (11), it suffices to measure independently the terms $(\rho_{AH}/\rho)^2$ and $\Delta\rho/2\rho$ on the Hall bar. The results measured on the Hall-bar devices patterned from the previous NiFe and GdCo multilayers are reported in Fig. 2. As expected [16], it can be seen that the magnetoresistance is dominated by the anisotropic magnetoresistance $\Delta R_{AMR}/R_{AMR}$ for the NiFe sample in Fig. 2(b) (transition metal ferromagnet), while it is dominated by the anomalous Hall effect $(\rho_{AH}/\rho)^2$ for the GdCo rare earth–transition metal alloys in Fig. 2(e). Figure 2(c) shows that the anomalous Hall effect is negligible in NiFe and Fig. 2(d) shows that the anisotropic Hall effect is negligible in GdCo. The insets in both figures are zooms with a magnification of 100×. Note that a small contribution of the AMR can also be present in the inset of Fig. 2(c) due to a slight misalignment of the electrodes (see Supplemental Material for a detailed study [19]).

More qualitatively, we deduce from Eq. (1) that, with homogeneous magnetization and current density, the anisotropic magnetoresistance (AMR), which is by definition measured longitudinally to the current (along x), reads

$$R_{AMR} = \frac{L}{wt}\left(\rho + \Delta\rho m_x^2\right), \tag{13}$$

where t is the thickness, L is the length, and w is the width of the Hall bar. Close to the magnetic saturation (at $B_z = 1$ T) the magnetization is almost aligned with the magnetic field, i.e., $m_x \approx 0$. At zero field the magnetization lies in the plane of the sample, aligned with the current direction ($m_x = 1$). Consequently, the AMR amplitude $\Delta R_{AMR}/R_{AMR}$ at the saturation field is equal to $\Delta\rho/\rho$. From Figs. 2(b) and 2(d), we can deduce the values of the parameters $\Delta\rho^{NiFe}/\rho^{NiFe} \approx 1.3 \times 10^{-2}$ and $\Delta\rho^{CoGd}/\rho^{CoGd} \approx 8.5 \times 10^{-5}$.

On the other hand, $R_{AH} \equiv E_y l/I$ is the anomalous Hall resistance defined by the voltage measured transversely (along y) divided by the current $I = J_x wt$ injected along x. The expression of E_y is deduced from Eq. (1),

$$R_{AH} = \frac{1}{t}\left(\frac{\Delta\rho}{\rho} m_x m_y + \frac{\rho_{AH}}{\rho} m_z\right). \tag{14}$$

The right-hand side of Eq. (14) defines the planar Hall magnetoresistance (first term) and the anomalous Hall magnetoresistance (last term). At saturation, the magnetization is aligned along the z direction, and we can rewrite Eq. (14) as $\frac{R_{AH}}{R} \approx \frac{\rho_{AH}}{\rho}\frac{\omega}{L}$, or $\frac{\rho_{AH}}{\rho} = \frac{R_{AH}\,t}{\rho}$. Since the resistivity ρ of the CoGd alloy is of the order of 120 $\mu\Omega$ cm and $t = 23$ nm, the measurement of the Hall bar then gives $\rho_{AH}/\rho \approx 1.6 \times 10^{-2}$. The results are summarized in Table I.

The comparison is excellent in the case of the NiFe (-6.5×10^{-3} instead of -6.7×10^{-3}), with a largely dominant contribution of the anisotropic magnetoresistance (the anomalous Hall contribution is negligible). On the other hand, the value of the anomalous Hall coefficient ρ_{AH}/ρ of GdCo is underestimated in the Hall-bar geometry (1.5×10^{-4} instead of 3.5×10^{-4}). This discrepancy can be understood by the 3-nm Pt cap layer (lower ρ measured in the Hall bar) and by the strong perturbation of the current lines due to the lateral contacts of Pt (higher ρ_{AH} measured in the Hall bar). Indeed, this problem is inherent in Hall-cross devices [8], and is one of the main motivations for the use of Corbino devices. In the last case, the two electrodes follow the radial geometry by imposing the radial voltage, in contrast to the former case, for which the electrodes break to translational invariance along the longitudinal axis. We observe nevertheless a good order of magnitude in the application of Eq. (12).

TABLE I. Comparison between the measured Corbino magnetoresistance and the Corbino coefficients $\mathcal{C}$ defined in Eq. (11) from the Hall-bar measurements.

Coefficients	NiFe	CoGd
$\Delta\rho/\rho$ [from Figs. 2(b) and 2(d)]	1.3×10^{-2}	8.5×10^{-5}
R_{AH} [from Figs. 2(c) and 2(e)]	$\lesssim 4 \times 10^{-3}\ \Omega$	$8 \times 10^{-1}\ \Omega$
$(\rho_{AH}/\rho)^2$	5×10^{-7}	2.35×10^{-4}
Corbino coeficient $\mathcal{C}$ [calculated from Eq. (11)]	-6.5×10^{-3}	1.5×10^{-4}
Corbino magnetoresistance (measured from Fig. 1)	-6.7×10^{-3}	3.5×10^{-4}

In conclusion, the magnetoresistance of Corbino disks of NiFe and GdCo has been measured as a function of magnetization direction. This observed Corbino magnetoresistance is interpreted in the framework of a phenomenological model, that allows the Corbino parameters to be expressed as a function of the usual Hall-bar parameters, which are the isotropic resistivity ρ, the anisotropic resistivity $\Delta\rho/\rho$, and the anomalous Hall resistivity ρ_{AH}. The typical negative (NiFe) or positive (GdCo) quadratic Corbino magnetoresistance observed with respect to the external magnetic field is explained by the competition between anisotropic magnetoresistance terms (negative contribution) and the anomalous Hall magnetoresistance (positive contribution).

This Rapid Communication shows that the magnetoresistance profiles between the Hall bar and the Corbino disks are due to the absence of Hall current in the former geometry, and the presence of the orthoradial spin-dependent Hall current in the latter geometry. This difference changed drastically the symmetry of the magnetoresistance, from negative to positive magnetoresistance observed between Figs. 1(c) and 2(b) for NiFe, and from even to odd magnetoresistance observed between Figs. 1(b) and 2(e) for GdCo. Similar effects are also expected in the context of the spin-Hall effect (e.g., using nonferromagnetic layers) while playing with the electrical properties of the interfaces, with potential applications in spin-to-charge conversion devices.

Financial funding RTRA *Triangle de la physique* Projects DEFIT No. 2009-075T and DECELER No. 2011-085T, the DGA project "Spin" CNV 2146, the FEDER, *La région Lorraine*, Le grand Nancy, ICEEL, and the ANR-12-ASTR-0023 Trinidad are greatly acknowledged. This work was also supported by the French PIA project Lorraine Université d' Excellence ANR-15-IDEX-04-LUE.

[1] E. H. Hall, On a new action of the magnet on electric currents, Am. J. Math. **2**, 287 (1879).

[2] O. M. Corbino, Electromagnetic effects due to distortions that a field produces on nonmetallic ion paths, Physik. Z. **12**, 561 (1911).

[3] E. Adams and A. K. Chapman, LXXII. The Corbino effect, London, Edinburgh Dublin Philos. Mag. J. Sci. **28**, 692 (1914).

[4] E. P. Adams, The Hall and Corbino effects, Proc. Am. Philos. Soc. **54**, 47 (1915).

[5] H. P. R. Frederikse and W. R. Hosler, Galvanomagnetic effects in n-type indium antimonide, Phys. Rev. **108**, 1136 (1957).

[6] C. A. Simmons, Influence of the Hall effect upon the transverse magnetoresistance in indium antimonide, J. Appl. Phys. **32**, 1970 (1961)

[7] D. R. Backer and J. P. Heremans, Linear geometrical magnetoresistance effect: Influence of geometry and material composition, Phys. Rev. B **59**, 13927 (1999).

[8] R. S. Popovic, *Hall Effect Devices*, 2nd ed. (IOP, Bristol, 2004).

[9] S. A. Solin, T. Thio, D. R. Hines, and J. J. Heremans, Enhanced room-temperature geometric magnetoresistance in inhomogeneous narrow-gap semiconductors, Science **289**, 1530 (2000).

[10] J.-E. Wegrowe, R. V. Benda, and J. M. Rubì, Conditions for the generation of spin current in spin-Hall devices, Europhys. Lett. **118**, 67005 (2017).

[11] J.-E. Wegrowe and P.-M. Dejardin, Variational approach to the stationary spin-Hall effect, Europhys. Lett. **124**, 17003 (2018).

[12] R. Benda, J. M. Rubi, E. Olive, and J.-E. Wegrowe, Towards Joule heating optimization in Hall devices, Phys. Rev. B **98**, 085417 (2018).

[13] N. Nagaosa, J. Sinova, S. Onoda, A. H. MacDonald, and N. P. Ong, Anomalous Hall effect, Rev. Mod. Phys. **82**, 1539 (2010).

[14] J. Sinova, S. O. Valenzuela, J. Wunderlich, C. H. Back, and T. Jungwirth, Spin Hall effects, Rev. Mod. Phys. **87**, 1213 (2015).

[15] T. McGuire and R. Potter, Anisotropic magnetoresistance in ferromagnetic 3D alloys, IEEE Trans. Magn. **11**, 1018 (1975).

[16] T. McGuire, R. Gambino, and R. Taylor, Galvanomagnetic effects in amorphous film alloys, IEEE Trans. Magn. **13**, 1598 (1977).

[17] J.-E. Wegrowe, D. Lacour, and H.-J. Drouin, Anisotropic magnetothermal transport and spin Seebeck effect, Phys. Rev. B **89**, 094409 (2014).

[18] B. Madon, D. Ch. Pham, D. Lacour, M. Hehn, V. Polewczyk, A. Anane, V. Cros, and J.-E. Wegrowe, Anomalous and planar Righi-Leduc effect in $Ni_{80}Fe_{20}$ ferromagnets, Phys. Rev. B **94**, 144423 (2016), Sec. II A.

[19] See Supplemental Material at http://link.aps.org/supplemental/10.1103/PhysRevB.98.220405 for the derivation of the transport equations and the characterization of the samples based on magnetoresistance properties.

[20] L. Onsager, Reciprocal relations in irreversible processes. II., Phys. Rev. **38**, 2265 (1931).

[21] S. R. De Groot and P. Mazur, *Non-Equilibrium Thermodynamics* (Dover Publication, IC, New York, 1984).